

# Structural and Magnetic Modulation of a Purely Organic Open Framework by Selective Guest Inclusion

Daniel MasPOCH,<sup>[a]</sup> Neus Domingo,<sup>[b]</sup> Nans Roques,<sup>[a]</sup> Klaus Wurst,<sup>[c]</sup> Javier Tejada,<sup>[b]</sup> Concepció Rovira,<sup>[a]</sup> Daniel Ruiz-Molina,<sup>\*[a]</sup> and Jaume Veciana<sup>\*[a]</sup>

**Abstract:** Solvent inclusion/evacuation caused variations in the structural and magnetic characteristics of the purely organic porous magnet based on the tricarboxylic-substituted PTMTC radical. Whereas no inclusion is observed for nonpolar solvents, the exposure of crystals of the  $\alpha$ -phase of PTMTC to vapors of polar organic solvents with hydrogen acceptor and/or donor functionalities, such as, ethanol, benzoic alcohol, *n*-decanol, THF, and DMSO results in the inclusion of these solvents in the highly polar tubular channels of the  $\alpha$ -phase. The resulting inclusion

compounds of formula PTMTC·*x*(guest) show several structural rearrangements, as confirmed by IR and XRPD (X-ray powder diffraction) measurements. The crystal transformations have been studied for a specific case: the PTMTC·EtOH adduct. The crystal structure reveals that included guest solvent molecules participate in the formation of new hydrogen bonds

with the carboxylic groups of PTMTC radicals, inducing the disruption of several direct hydrogen bonds among these radicals. As expected, the interruption of direct hydrogen bonds between PTMTC radicals induces large transformations in the magnetic properties. From the ferromagnetic behavior of the  $\alpha$ -phase, predominant anti-ferromagnetic interactions are observed for the inclusion adducts. Interestingly, both structural and magnetic changes are reversible after removal of guest solvent molecules.

**Keywords:** host–guest systems • hydrogen bonds • magnetic properties • radicals • solvatomagnetism

## Introduction

Multitopic organic building blocks with selected geometries represent an excellent tool to resolve one of the most challenging issues facing supramolecular chemistry today, the


construction of crystalline porous molecular materials.<sup>[1]</sup> Following this strategy, excellent results have been obtained in the design of zeolite-like metal-organic robust open-framework structures, with a huge range of pore sizes (2–30 Å)<sup>[2]</sup> and unprecedented topologies.<sup>[3]</sup> Even more interesting is the possibility to add new properties to these structures besides their inherent porous character, which should facilitate multifunctionality of these systems.<sup>[1a,4]</sup> Indeed, the puzzled construction of metal-organic open frameworks allows the exploration of novel structural/dynamic characteristics, as well as physical functions, such as, chirality,<sup>[5]</sup> electrical,<sup>[6]</sup> optical,<sup>[7]</sup> or magnetic.<sup>[8,10–15]</sup> Among them, attainment of functional magnetic and/or dynamic structural porous solids is attracting considerable effort worldwide.<sup>[8,9]</sup> Magnetic porous solids have the potential to produce low-density magnetic materials or to develop multifunctional materials thanks to their capacity to encapsulate other functional molecular systems possessing additional conducting, optical, chiral, or nonlinear optical (NLO) properties. Thus far, ferromagnetic,<sup>[10]</sup> antiferromagnetic,<sup>[11]</sup> spin-frustration,<sup>[12]</sup> spin-crossover,<sup>[13]</sup> metamagnetic,<sup>[14]</sup> or ferromagnetic<sup>[15]</sup> behavior have been introduced in porous structures. On the other hand, coordination polymers with dynamic pores open new

[a] Dr. D. MasPOCH,<sup>†</sup> Dr. N. Roques, Prof. C. Rovira, Dr. D. Ruiz-Molina, Prof. J. Veciana  
Institut de Ciència de Materials de Barcelona, CSIC  
Campus Universitari de Bellaterra, 08193, Bellaterra (Spain)  
Fax: (+34)93-580-5729  
E-mail: dani@icmab.es  
vecianaj@icmab.es

[b] Dr. N. Domingo, Prof. J. Tejada  
Facultat de Física, Universitat de Barcelona  
Diagonal 647, 08028, Barcelona (Spain)

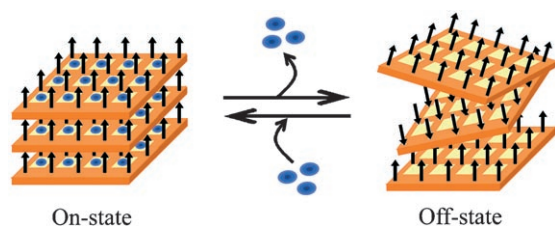
[c] Dr. K. Wurst  
Institute für Allgemeine, Anorganische und Theoretische Chemie  
Universität Innsbruck, Innrain 52<sup>a</sup>, 6020, Innsbruck (Austria)

[<sup>†</sup>] Current address: Institut Català de Nanotecnologia  
Campus Universitari de Bellaterra, 08193, Bellaterra (Spain)

 Supporting information (crystal structures of the  $\alpha$ - and  $\beta$ -phases, and inclusion studies (thermogravimetry and infrared spectra) of ethanol, benzoic alcohol, and THF in the  $\alpha$ -phase) for this article is available on the WWW under <http://www.chemeurj.org/> or from the authors.

routes to design highly selective porous solids. For instance, Fujita, Suh, and co-workers have recently described some examples of porous structures with modified crystal structure after a chemical and/or physical stimulus.<sup>[16,17,18]</sup> Generally, this property comes from the structural ability to suffer reversible structural modifications after selective sorption/desorption of solvent guest molecules.

In view of the excellent results previously described and to further expand the range of multifunctional porous materials, the possibility has recently been suggested to combine both the dynamic flexibility of open-framework coordination polymers with additional magnetic properties. Dynamic flexible open frameworks are interesting because of their capability to undergo reversible structural modifications by removal/sorption of solvent guest molecules. As the magnetic properties are closely dependent on the structure of the material, it is expected that reversible structural readjustments will induce a modulation of their magnetic properties. Therefore, by controlling the presence/absence of solvent guest within the porous structure, we may reversibly switch the magnetic properties within two states. For example, an “off/state” may be attained when the material is evacuated, whereas an “on/state” may be achieved when the material is filled (see Scheme 1). Such switchable behavior together



Scheme 1. Idealistic schematic representation of the solvatomagnetic behavior of a porous solid induced by the dynamic structural flexibility of its open framework.

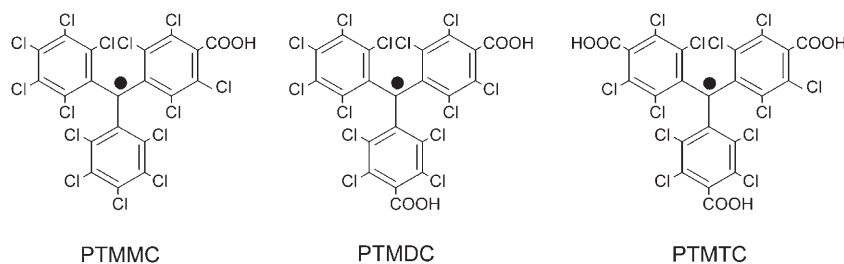
with the intrinsic high selective sorption properties associated with dynamic structural coordination polymers provides the ideal scenario to build potential selective molecular-based porous sensors for many gases or liquids.

Thus far, different examples of dynamic porous metal-organic solids with solvatomagnetic effects have been described. In 2002, Kepert and co-workers reported a dynamic porous coordination polymer with reversible spin-crossover phenomena by elongation and constriction of the pores caused by evacuation/reabsorption of alcohol solvent molecules.<sup>[11]</sup> Later, Kobayashi, Kurmoo and co-workers reported several examples of porous magnets with very interesting reversible solvatomagnetic effects.<sup>[19]</sup> For example,  $[\text{Co}_3(\text{OH})_2-$

$(\text{C}_2\text{O}_4)_2] \cdot 3\text{H}_2\text{O}$  shows reversible dehydration/rehydration followed by the interconversion from ferromagnetic to anti-ferromagnetic ordering.<sup>[20]</sup> More recently, some Prussian Blue analogues that exhibit both solvatomagnetic and solvatochromic effects upon a dehydration/hydration process have also been described by Ohkoshi, Hashimoto and co-workers.<sup>[21]</sup> In our group, we also reported a porous two-dimensional molecular coordination polymer, MOROF-1, which exhibits striking changes in its crystal structure, from an amorphous state when it is evacuated, to a crystalline state when it is selectively filled with ethanol or methanol solvent guest molecules.<sup>[22]</sup> As a consequence, the magnetic critical temperature is modulated from 0.4 to 2–3 K when MOROF-1 is evacuated or filled, respectively.

All the examples previously described involve the use of paramagnetic transition-metal ions that confer a magnetic character to the open-framework structure. However, as far as we know, there are no previous examples of a pure organic open-framework structure exhibiting solvatomagnetic effects. In fact, the acquisition of pure organic magnetic porous materials has remained elusive for long time. Even though several examples of pure organic open-framework systems were previously described,<sup>[23,24,25]</sup> none of them exhibited magnetic properties due to the lack of transition-metal ions and the diamagnetic character of the organic molecular building blocks used thus far. To circumvent all these problems, a few years ago we initiated a new approach for the preparation of magnetic porous materials based on the use of open-shell molecules<sup>[26]</sup> as multitopic organic synthons.<sup>[27]</sup> Such a family of ligands is that based on carboxylic-substituted polychlorotriphenylmethyl radicals (PTM; Scheme 2).

The advantages of this PTM family of radicals are manifold: 1) These bulky radicals are sterically hindered due to the presence of several chlorine atoms, which renders them thermally and chemically stable, but also prevents close packing and interpenetration within the final structure;<sup>[28]</sup> 2) carboxylic-PTM radicals are open-shell species capable of transmitting and increasing magnetic interactions through the structure, as previously shown for PTMMC,<sup>[29]</sup> which formed hydrogen-bonded  $\text{R}^2_2(8)$  dimers that promoted the transmission of a weak ferromagnetic interaction; and 3) carboxyl-substituted PTM radicals can be considered as an expanded version of trimesic acid, in which the benzene-1,3,5-triyl units have been replaced by an  $\text{sp}^2$ -hybridized



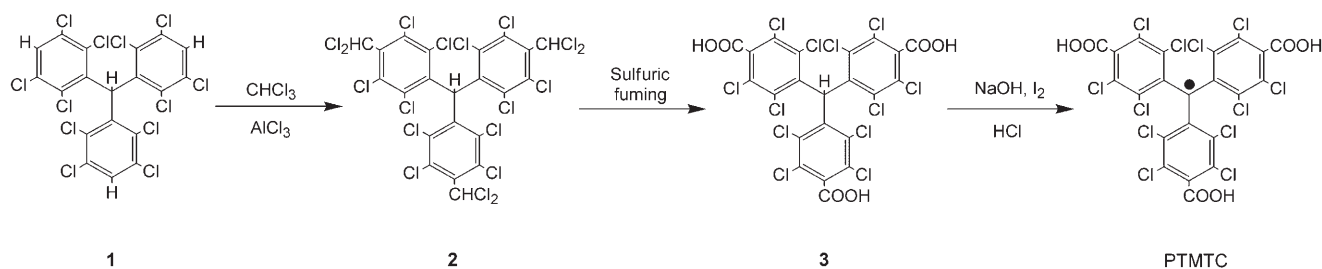
Scheme 2. Carboxylic-substituted polychlorinated triphenylmethyl radicals.

carbon atom decorated with three polychlorophenyl rings substituted with carboxylic acid groups.<sup>[22]</sup>

Following this strategy, a few years ago we reported the first example of a purely organic magnetic material with a robust open framework based on the supramolecular arrangement of an open-shell dicarboxylic perchlorinated triphenylmethyl (PTMDC) radical.<sup>[26a]</sup> However, no solvato-magnetic effects were observed for this structure. Herein, we report the detailed synthesis of radical PTMTC and its corresponding supramolecular packing, which will be referred to from now on as  $\alpha$ -phase or POROF-2 (POROF stands for purely organic radical open framework). The  $\alpha$ -phase combines a robust open-framework structure with magnetic ordering at low temperatures. The highly polar void volume due to the hydrogen-bonded porous network provides a unique environment to promote the selective inclusion of polar organic solvents with hydrogen-donor or -acceptor functionalities, which strongly influence its crystal structure and magnetic properties.<sup>[30]</sup> The structural transformations experienced by the hydrogen-bonded network of the  $\alpha$ -phase after inclusion of solvent guest molecules will be studied by using a specific case, the inclusion of ethanol molecules.

## Results and Discussion

**Synthesis:** The preparation of radical PTMTC was carried out following a four-step procedure outlined in Scheme 3. Tris(2,3,4,5-tetrachlorophenyl)methane (**1**) was synthesized according to the well-documented method found in the literature.<sup>[31]</sup> Three dichloromethyl groups were introduced into **1** by reacting it with anhydrous chloroform following a Friedel–Crafts reaction under high pressure at 160 °C for 8 h. The resulting molecule **2** was treated with fuming sulfuric acid at 150 °C for 12 h. At high temperatures, 20% fuming sulfuric acid hydrolyzes and subsequently oxidizes the dichloromethyl groups of **2** to carboxylic groups to furnish triacid **3**. Finally, treatment of the hydrocarbon precursor **3** with sodium hydroxide in DMSO gave a red solution of the tricarboxylate carbanion, which was later oxidized to the tricarboxylate radical in the presence of iodine and finally acidified with HCl to obtain radical PTMTC. The PTMTC radical is a stable species both in solution and in the solid state, and it was characterized by different techniques, such



Scheme 3. Synthesis of the PTMTC radical.

as, elemental analysis, ESI-TOF/MS, FT-IR, and EPR spectroscopies.

**X-ray structure of the  $\alpha$ -phase of PTMTC:** Crystallization by slow diffusion of pure *n*-hexane into a solution of PTMTC in dichloromethane gave red hexagonal plate crystals of the  $\alpha$ -phase or POROF-2. Single crystals of the  $\alpha$ -phase suitable for single X-ray diffraction analysis were also obtained by a slow evaporation of a solution of PTMTC in dichloromethane and *n*-hexane in 2:1 ratio.

Radical PTMTC crystallizes in the  $\alpha$ -phase in the trigonal  $P\bar{3}c1$  group with  $Z=4$  (Table 1). An ORTEP representation

Table 1. Crystallographic data for the  $\alpha$ -phase and  $\beta$ -phase of PTMTC.

	$\alpha$ -phase	$\beta$ -phase
formula	$C_{22}H_3Cl_{12}O_6$	$C_{24}H_{11}Cl_{12}O_8$
$F_w$	788.64	852.73
crystal system	trigonal	triclinic
space group	$P\bar{3}c1$	$P\bar{1}$
$a$ [Å]	15.9283(7)	8.7737(4)
$b$ [Å]	15.9283(7)	13.3814(8)
$c$ [Å]	13.8886(11)	14.4784(8)
$\alpha$ [°]	90.00	68.519(3)
$\beta$ [°]	90.00	79.629(3)
$\gamma$ [°]	120.00	88.026(3)
$V$ [Å <sup>3</sup> ]	3051.6(3)	1554.99(11)
$Z$	4	2
$T$ [K]	233(2)	233(2)
$R_1$	0.0585	0.0512
$wR_2$	0.1418	0.1154
GOF	1.133	1.035

of the molecular conformation is shown in Figure 1. As can be observed, it adopts the typical propeller-like conformation usually found in this family of radicals, which is defined by the dihedral angles, with values in the range of 44–56°, between the mean planes of each of the three polychlorinated aromatic rings and the reference plane, formed by the three bridgehead carbon atoms and the methyl one.<sup>[32]</sup> The high molecular symmetry on the crystal lattice is reflected by the presence of a  $C_3$  symmetry axis that crosses through the central carbon (C8) of PTMTC. Thus, the three polychlorinated aromatic rings are identical with a dihedral angle of 50°. Carboxylic groups are found to present a *syn*-planar conformation.<sup>[33]</sup> As was previously observed for PTMMC, the plane of the carboxylic groups lies orthogonal to that of the aromatic ring (87°) due to the great steric hin-

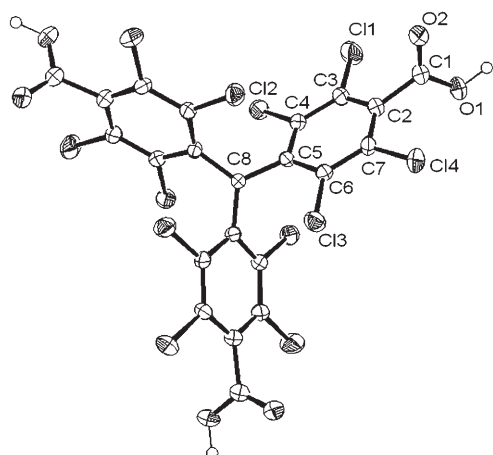


Figure 1. ORTEP plots at 50% of probability of PTMTC radical in the  $\alpha$ -phase.

drance of the chlorine atoms in *ortho* positions with respect to the carboxylic group.<sup>[34]</sup>

As far as the supramolecular packing is concerned, the PTMTC radical arranges in a large hexameric  $R_6^6(24)$  motif (Figure 2a), similar to that observed for the dicarboxylic PTMDC radical.<sup>[26a]</sup> This  $R_6^6(24)$  centrosymmetric cyclic motif adopts a nearly planar arrangement formed by six mutually hydrogen-bonded carboxylic groups of PTMTC radicals with O1...O2 distances of 2.657 Å and O-H...O angles

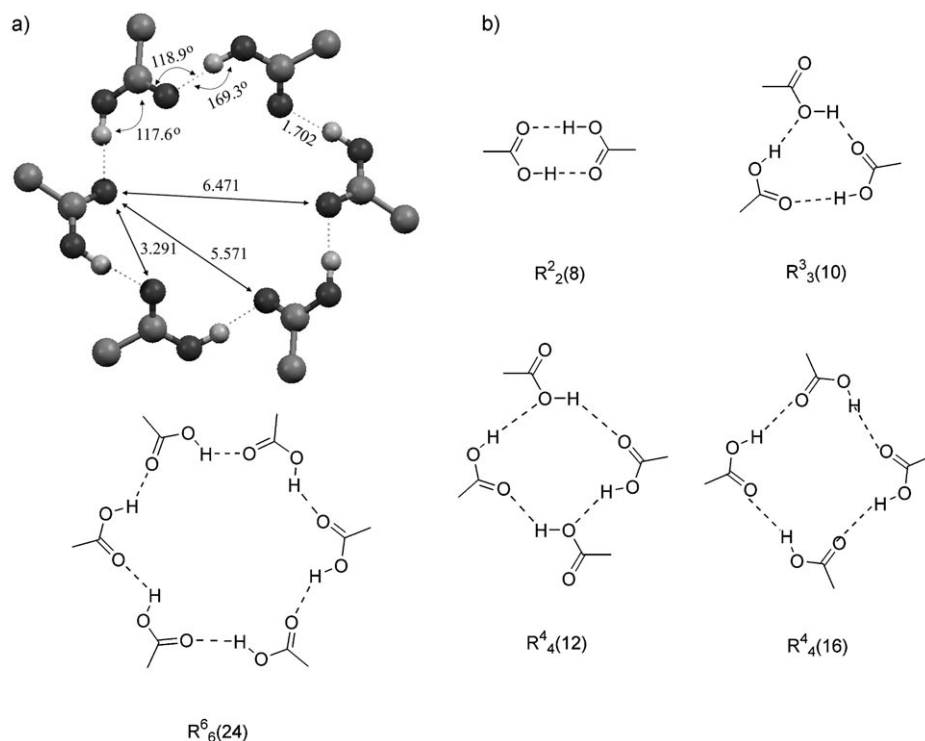


Figure 2. a) Geometrical characteristics of the hexameric  $R_6^6(24)$  ring formed by intermolecular hydrogen bonds of six PTMTC radicals. Distances are in Å. b) Cyclic hydrogen-bonded carboxylic patterns found for other organic carboxylic acids.

of 169° (for more details of the geometry, see Figure 2). Such a motif is a very rare case among the hydrogen-bonded supramolecular structures based on carboxylic groups, and probably it is associated with the rigidity and bulkiness of these PTM radicals. Indeed, one of the most frequent and dominant hydrogen-bonded motifs is the *syn-syn* centrosymmetric  $R_2^2(8)$  dimer.<sup>[33,35]</sup> However, other patterns in the form of infinite noncyclic hydrogen-bonded catemer motifs and even rarer cyclic trimeric and tetrameric motifs have also been found.<sup>[36]</sup> In fact, a crystallographic search done by us by using the Cambridge Structural Database (CSD, version 5.28, November 2006) confirmed that the largest hydrogen-bonded cyclic motif found, exclusively formed by carboxylic groups, is the unusual tetrameric  $R_4^4(16)$  motif.<sup>[37]</sup> For the sake of clarity, a representation of the different hydrogen-bonded motifs found for carboxylic groups is shown in Figure 2b.

The participation of each PTMTC radical in the formation of three identical hydrogen-bonded  $R_6^6(24)$  hexameric motifs leads to the formation of a two-dimensional hydrogen-bonded plane, in which each hexameric unit is hydrogen-bonded to six identical motifs along the *ab* plane (Figure 3a). The proper pillared packing of these hydrogen-bonded layers creates an open-framework structure. ABAB alternation of the layers along the *c* axis generates a three-dimensional structure that exhibits tubular channels, where a sphere 5.2 Å in diameter can fit inside them (Figure 3b). Indeed, the columnar disposition of hydrogen-bonded hexameric units creates highly hydrophilic tubular channels with solvent-accessible voids that amount up to 15% (450 Å<sup>3</sup> per unit cell) of the total volume. Further weaker supramolecular interactions stabilize the overall structure. Among them, several Cl...Cl contacts (six per molecule) stabilize each hydrogen-bonded sheet, whereas six additional Cl...Cl contacts per molecule link adjacent layers.

**Structural rigidity of the  $\alpha$ -phase:** As stated above, the single-crystal X-ray diffraction study of the  $\alpha$ -phase showed the lack of guest solvent molecules within the tubular channels of the open-framework structure. This fact has been confirmed by elemental analysis and thermogravimetric (TG) studies.<sup>[38]</sup> As can be seen in Figure 4, thermogravimetric analysis of a few single crystals of the  $\alpha$ -phase showed no weight loss in the temperature range of 25 to 250°C. More-



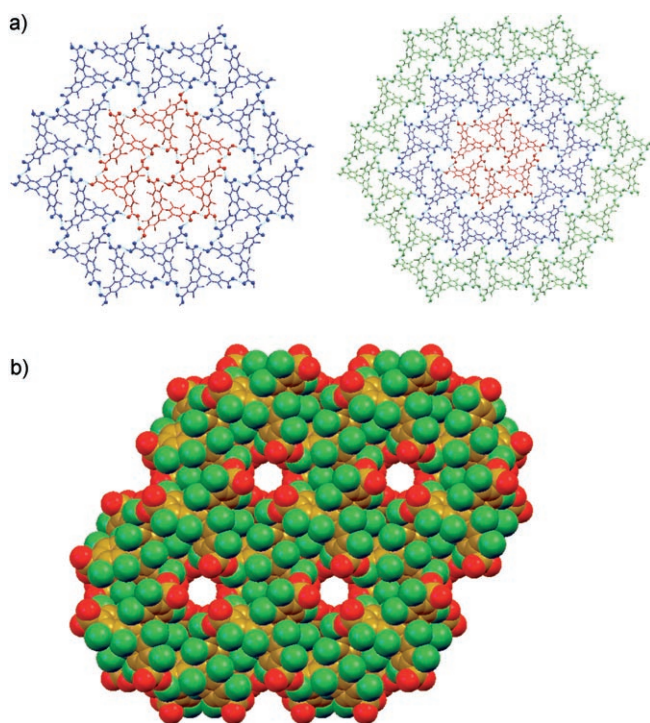


Figure 3. a) Stepwise growth of the two-dimensional hydrogen-bonded sheets in  $\alpha$ -phase; b) space-filling representation showing the tubular channels of the  $\alpha$ -phase.

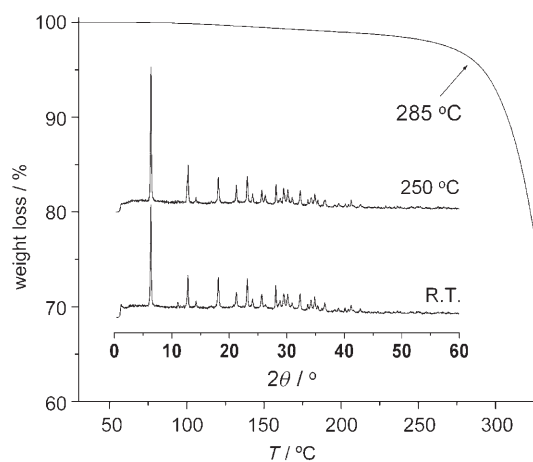


Figure 4. Thermal behavior of the as-synthesized  $\alpha$ -phase and (inset) comparison of the XRPD patterns for the as-synthesized and heated materials.

over, XRPD experiments over such a temperature range, shown in Figure 4, also showed that positions and intensities of all lines remain unchanged when compared with the XRPD pattern of an as-synthesized sample, confirming not only the lack of guest solvent molecules, but also that the  $\alpha$ -phase has a high structural rigidity because it does not collapse when heated up to 250 °C. Finally, a further increase of the temperature above 285 °C led to the decomposition of the PTMTC, as confirmed by combined XRPD and FT-IR characterization.

In addition to the highly robust hydrogen-bonded network, the large number of chlorine atoms present in the skeleton of the tricarboxylic PTMTC radicals has significant implications for such structural stability. Indeed, both stabilization of the crystal structure through the formation of multiple Cl $\cdots$ Cl contacts in the solid state and the remarkable steric congestions due to bulky chlorine atoms, may be the main reason for obtaining noncatenated crystal packing<sup>[39]</sup> in spite of the Kitaigorodski principle of close packing.

**Inclusion properties of the  $\alpha$ -phase:** The absence of solvent guest molecules within the tubular pores provides an approximate free pore volume of around 15% of the total volume cell. This highly polar potentially accessible void volume combined with its high thermal stability up to 250 °C are well known optimum conditions to consider  $\alpha$ -phase as a good candidate to selectively include certain solvent guest molecules and, therefore, to behave as a purely organic “zeolite-like” material. In such a context, to study the guest-exchange properties of the  $\alpha$ -phase, we performed a series of solid–gas experiments in which crystals of as-synthesized  $\alpha$ -phase were introduced into a sealed vessel containing the liquid solvent and placed in equilibrium with its vapor for 48 h.

Interestingly, the  $\alpha$ -phase does not exhibit guest-exchange behavior in contact with vapor of “nonpolar” solvents, such as *n*-hexane, dichloromethane, chloroform, benzene, or toluene. Similar results were obtained by dipping crystals of  $\alpha$ -phase directly into liquid solutions of *n*-hexane, chloroform, toluene, and carbon tetrachloride for 48 h, which do not show any sign of sorption. This lack of affinity for nonpolar solvents is most likely due to the highly polar environment character of the channels in the  $\alpha$ -phase, and agrees with its solvent-free structure. Accordingly, exposure to solvent vapors of polar organic solvents with hydrogen acceptor and/or donor functionalities, such as ethanol (EtOH), benzoic alcohol (Bz-CH<sub>2</sub>-OH), *n*-decanol (C<sub>10</sub>H<sub>22</sub>O), tetrahydrofuran (THF), and dimethyl sulfoxide (DMSO) leads to the formation of different adducts or inclusion compounds of the formula PTMTC·*x*(guest), as evidenced by combined elemental analysis, IR spectroscopy, and TG studies. In this case, a direct contact with the liquid was not possible because the PTMTC radical is very soluble in these solvents at room temperature. A summary of the results obtained with different polar solvents is shown in Table 2.

As can be seen in Table 2, elemental analysis and FT-IR spectra of all inclusion compounds or adducts confirmed the presence of solvent molecules with different host–guest stoichiometries. For instance, the FT-IR spectra of an as-synthesized sample of  $\alpha$ -phase and a few selected adducts are shown in the Supporting Information. Close examination of the FT-IR spectra shows the characteristic bands of both the PTMTC host radical and solvent guest bands as indicated below: 1) EtOH bands at 2979, 1455, and 1377 cm<sup>-1</sup> for PTMTC·EtOH; 2) benzyl alcohol bands at 3030, 1454, 1207, and 700 cm<sup>-1</sup> for PTMTC·0.5 BzCH<sub>2</sub>OH; 3) *n*-decanol bands at 2926, 1466, and 1301 cm<sup>-1</sup> for PTMTC·0.6 C<sub>10</sub>H<sub>22</sub>O; 4) THF bands at 2974, 1462, 1292, 915, and 877 cm<sup>-1</sup> for

Table 2. Results of inclusion studies on crystals of the  $\alpha$ -phase of PTMTC and the resulting characterization data of PTMTC adducts.

Adducts	Elemental analysis	Weight loss in TG	IR [ $\text{cm}^{-1}$ ]
PTMTC·EtOH	found: C 34.39 %, H 0.88 % calcd: C 34.54 %, H 1.08 %	found: 5.0 % (from 50 to 175 °C) calcd: 5.5 %	2979, 1455, 1377
PTMTC·0.5 BzCH <sub>2</sub> OH	found: C 36.57 %, H 1.01 % calcd: C 36.32 %, H 0.83 %	found: 5.8 % (from 50 to 115 °C) calcd: 6.5 %	3030, 1454, 1207, 700
PTMTC·0.6 C <sub>10</sub> H <sub>22</sub> O	found: C 37.82 %, H 1.66 % calcd: C 38.06 %, H 1.83 %	found: 10.8 % (from 90 to 120 °C) calcd: 10.7 %	2926, 1466, 1301
PTMTC·THF	found: C 36.49 %, H 0.82 % calcd: C 36.28 %, H 1.28 %	found: 9.0 % (from 75 to 130 °C) calcd: 8.4 %	2974, 1462, 1292, 915, 877
PTMTC·2DMSO	found: C 33.39 %, H 1.04 % calcd: C 33.48 %, H 1.61 %	found: 16.8 % (from 75 to 225 °C) calcd: 15.4 %	2996, 1435, 1014, 947, 671

PTMTC·THF, and; 5) DMSO bands at 2996, 1435, 1014, 947, and 671  $\text{cm}^{-1}$  for PTMTC·2DMSO. At this point, it is also worth mentioning that in addition to the presence of the solvent bands, significant changes in the bands around 1750–1650  $\text{cm}^{-1}$ , attributed to the asymmetric and symmetric C=O stretching vibrations of the carboxylic groups, were observed. For instance, FT-IR spectra of the as-synthesized  $\alpha$ -phase show the two bands of the carboxylic groups at 1722 and 1678  $\text{cm}^{-1}$ . However, when solvent guest molecules are included, the first band increases in intensity and shifts to higher values (1739–1727  $\text{cm}^{-1}$ ), whereas the second band shifts to values around 1660–1693  $\text{cm}^{-1}$ . This fact may indicate that the hydrogen-bonded network of the  $\alpha$ -phase experiences conformational readjustments with the inclusion of guest solvent molecules. Such conformational readjustments were confirmed by XRPD experiments. Indeed, the XRPD pattern for the solvent adducts exhibited different peaks from those observed for an as-synthesized sample of  $\alpha$ -phase (Figure 5).

Even more interesting was the reversible removal of the guest solvent molecules and the recovery of the initial crystalline structure of the  $\alpha$ -phase. Indeed, as can be seen in Table 2 and in the Supporting Information, thermogravimetric studies performed on the resulting polycrystalline PTMTC· $x$ (guest) adducts revealed that all of solvent guest molecules can be evacuated from the channels at temperatures not higher than 250 °C. Moreover, the crystal structure of the  $\alpha$ -phase is mostly recovered after removal of included solvent guest molecules as confirmed by: 1) the resulting material for all the evacuated crystals can be elucidated by elemental analysis as PTMTC; 2) their XRPD patterns are in perfect agreement with that of an as-synthesized sample of guest-free  $\alpha$ -phase (see Figure 5); and 3) FT-IR spectra for evacuated samples reveal the C=O bands characteristic of  $\alpha$ -phase at 1722 and 1667–1668  $\text{cm}^{-1}$  are re-established (see Supporting Information). The reversibility of this process was further confirmed by recycling the evacuated  $\alpha$ -phase for additional solvent inclusion experiments.

**Structural readjustments in PTMTC·EtOH adduct: the new  $\beta$ -phase of PTMTC:** To confirm the structural transformations experienced by the porous network of the  $\alpha$ -phase after inclusion of solvent molecules, we first attempted the crystal structure resolution of some of the inclusion PTMTC· $x$ (guest) compounds. However, the poor quality of

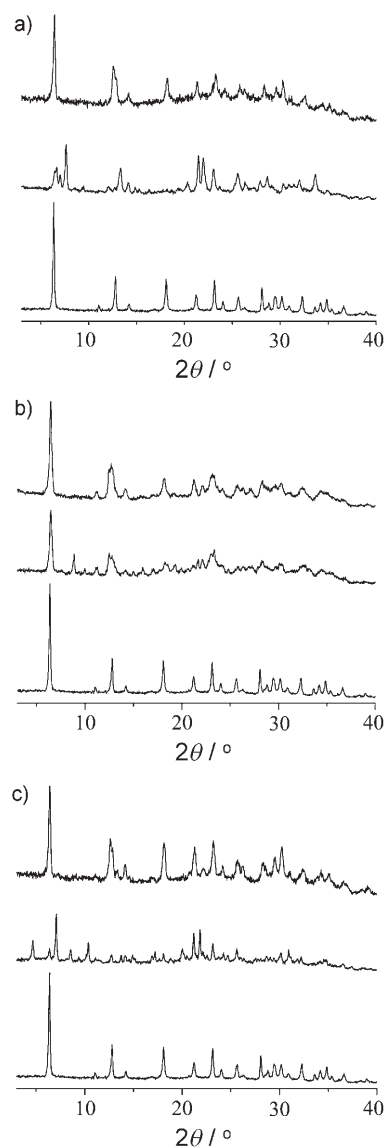


Figure 5. XRPD studies of the reversible structural rearrangements experienced within the hydrogen-bonded network of the  $\alpha$ -phase with incorporated: a) ethanol, b) benzyl alcohol, and c) THF. In these studies, the bottom, medium, and top spectra correspond to the initial guest-free as-synthesized  $\alpha$ -phase material, vapor-exposed  $\alpha$ -phase, and evacuated  $\alpha$ -phase, respectively.

the resulting inclusion crystals prevented us from solving any of those crystal structures except in the case of ethanol. We then focused our attention on the study of the inclusion of ethanol molecules by performing a direct crystallization of an as-synthesized sample of the  $\alpha$ -phase in ethanol. The idea was the preparation of a new crystalline phase with a structure similar to that of the PTMTC·EtOH adduct. Therefore, a microcrystalline as-synthesized sample of the  $\alpha$ -phase was first dissolved in ethanol, and the resulting solution was slowly evaporated for seven days to give red prismatic crystals of a new crystalline  $\beta$ -phase (Table 1). The XRPD pattern obtained for the PTMTC·EtOH adduct was then compared with that obtained for the  $\beta$ -phase. As can be seen in Figure 6, the  $\beta$ -phase of PTMTC shows an

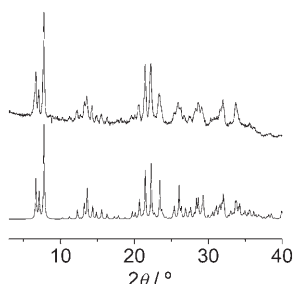


Figure 6. Comparison of the simulated XRPD pattern of  $\beta$ -phase (bottom) and experimental XRPD of PTMTC·EtOH adduct (top).

identical XRPD pattern to that of a polycrystalline sample of the inclusion PTMTC·EtOH adduct, and confirms that both crystalline samples are isostructural. This fact, together with the chemical shifts observed in the IR spectra for the band characteristics of the carboxylic groups, led us to believe that the structural rearrangements originating from the inclusion of ethanol guest molecules in the  $\alpha$ -phase could be understood by simply comparing both  $\alpha$ - and  $\beta$ -phases.

If one compares both crystal structures, the major difference is the presence of solvent guest molecules inside the channels that interact through hydrogen bonds with the carboxylic groups of PTMTC radicals forming the inner walls of these channels (Figure 7). From these interactions, direct hydrogen bonds between PTMTC radicals are broken, and

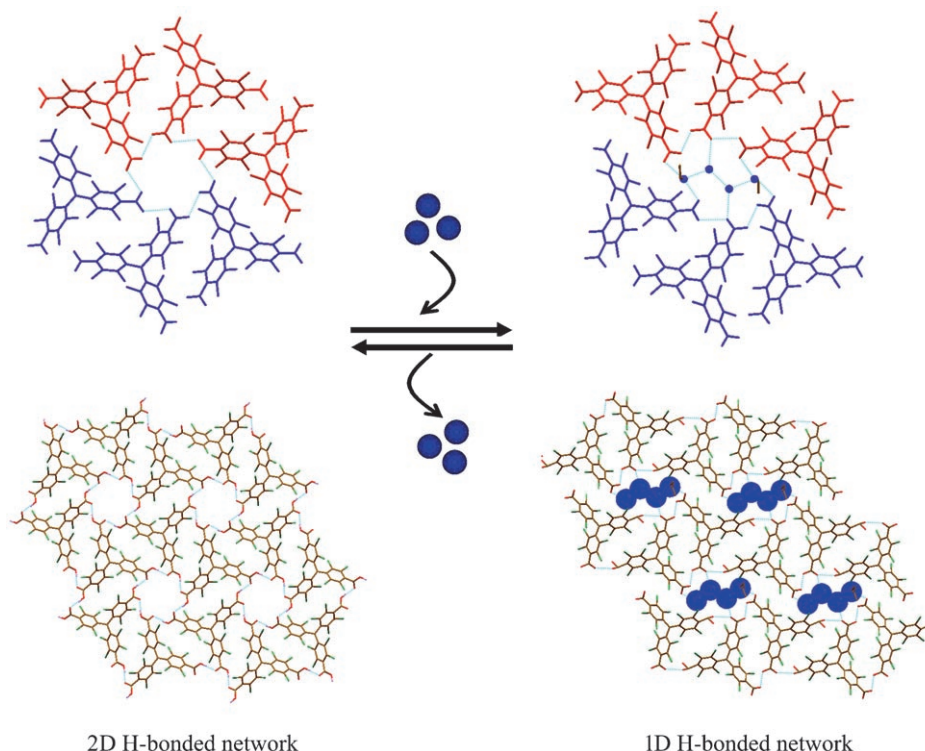


Figure 7. Comparison between crystal structures of  $\alpha$ - and  $\beta$ -phases, showing the structural rearrangement experienced by the hydrogen-bonded network of the  $\alpha$ -phase with incorporated ethanol solvent molecules.

the repetitive cyclic  $R_6^6(24)$  hexameric motif is divided into two hydrogen-bonded trimers formed by three carboxylic groups linked through two hydrogen bonds ( $O1\cdots O4$  and  $O3\cdots O6$ ) with bond lengths of 2.591 and 2.75 Å, respectively. Besides the disruption and enlargement of each  $R_6^6(24)$  hexamer, these new trimers are also slightly displaced along one direction (see Figure 7 top). The disruption of direct hydrogen bonds between PTMTC radicals has also an effect on the long-range hydrogen-bonded assembly of these radicals. Indeed, as shown in Figure 7 bottom, the two-dimensional layers of hydrogen-bonded PTMTC radicals in the  $\alpha$ -phase are reduced to one-dimensional chains that run along the [110] axis. Now, these chains are connected to each other by solvent molecules to form a two-dimensional hydrogen-bonded sheet along a plane with the vectors [110] and [101].

**Magnetic properties:** As we have already described for the monocarboxylic PTMMC radical,<sup>[29]</sup> hydrogen bonds between carboxylic groups are capable of transmitting weak ferromagnetic interactions. However, when these supramolecular interactions are broken, ferromagnetic exchange interactions are also disrupted. As state above, the  $\alpha$ -phase has the ability to incorporate solvent molecules by inducing large structural changes on its crystal structure. In the case of the PTMTC·EtOH adduct, the reversible solvent-induced dynamic structural changes involve the disturbance of some direct hydrogen bonds between PTMTC radicals and, therefore, changes in the magnetic properties should be expected. These expectations prompted us to study in detail the mag-

netic properties of  $\alpha$ -phase and its related adduct to observe possible solvatomagnetic effects.

**Magnetic properties of  $\alpha$ -phase:** Temperature dependence of magnetic susceptibility of a polycrystalline sample of  $\alpha$ -phase was measured from 300 to 1.8 K in a SQUID magnetometer (Figure 8a). The temperature was further decreased to 70 mK by using a dilution cryostat (Figure 8b).

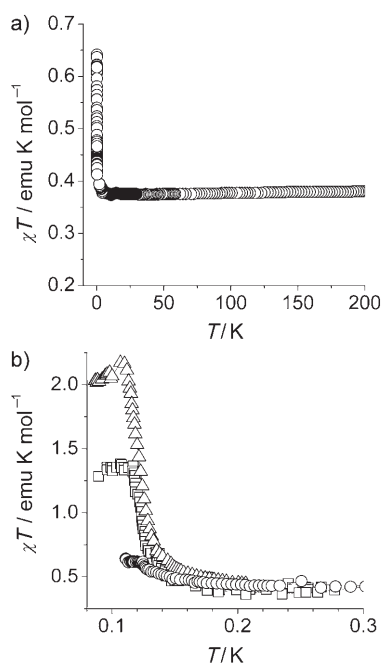


Figure 8. a) Temperature dependence of  $\chi \cdot T$  product for a polycrystalline sample of the  $\alpha$ -phase in the range of 0.1 to 300 K, measured under an applied magnetic field of 1000 Oe; b) temperature dependence of the  $\chi \cdot T$  product at very low temperatures, measured under different applied magnetic fields:  $H = 200$  Oe ( $\Delta$ ), 500 Oe ( $\square$ ), 1000 Oe ( $\circ$ ).

As can be seen in Figure 8a, the magnetization of this hydrogen-bonded network of the  $\alpha$ -phase follows a typical Curie–Weiss behavior in the range from 300 to 10 K. In fact, the data was successfully fitted by using the law  $\chi_M = \frac{C}{(T-\theta)} \equiv \frac{N\beta^2 g^2}{2k_B(T-\theta)}$  with  $C = 0.38$  emu K mol $^{-1}$  and a Weiss constant of  $\theta = +0.2$  K. The  $\chi \cdot T$  product had a value of 0.38 emu K mol $^{-1}$  at 300 K, as expected for uncorrelated  $S = 1/2$  spins, which also confirms the purity of this sample. Below 10 K, magnetic measurements performed with the  $\alpha$ -phase show that  $\chi T$  value increases on decreasing the temperature up to a maximum around 110 mK, followed by a plateau. This peak indicates the long-range ordering of the magnetic moments.<sup>[40]</sup> Moreover, the intensity of the peak decreases on increasing the external applied magnetic field as shown in Figure 8b. For instance, for an applied magnetic field of 200 Oe a value of 2.2 emu K mol $^{-1}$  was obtained, whereas for an external field of 500 Oe the value reduced to 1.4 emu K mol $^{-1}$ ; thus, obeying a saturation of the magnetization on increasing the applied magnetic field.

The transition to a ferromagnetic ordered state at very low temperatures was also confirmed by isothermal magnetization curves measured above and below the critical temperature (Figure 9). Whereas at 1.35 K, the  $\alpha$ -phase remains

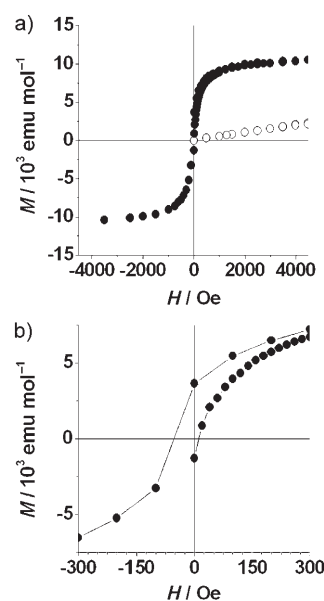


Figure 9. a) Isothermal field dependence of the magnetization for  $\alpha$ -phase at 1.35 K ( $\circ$ ) and 80 mK ( $\bullet$ ); b) the hysteresis cycle at 80 mK.

in the paramagnetic region and therefore the magnetization curve has a slight gradient, the curve at 80 mK, even though it is very close to the critical temperature, traces a hysteresis loop characteristic of a soft ferromagnet, with a sharp increase of the magnetization with the applied magnetic field that is almost saturated at about 400 Oe. The hysteresis loop for the  $\alpha$ -phase at 80 mK has a coercive field of the order of 50 Oe, and a remnant magnetization at zero field of about 35% of the saturation value.

**Magnetic properties of PTMTC-EtOH adduct:** The temperature dependence of the magnetic susceptibility of a polycrystalline sample of PTMTC-EtOH is shown in Figure 10. As for the  $\alpha$ -phase, this new crystalline phase shows paramagnetic behavior in the temperature range from 50 to 300 K, with a  $\chi \cdot T$  product value of 0.38 emu K mol $^{-1}$  at 300 K. However, on decreasing the temperature, the  $\chi \cdot T$  value slightly decreases according to the presence of very weak antiferromagnetic interactions. Experimental magnetic data was fit to the Curie–Weiss law with  $C = 0.38$  emu K mol $^{-1}$  and a Weiss constant of  $\theta = -0.4$  K. As expected, magnetic measurements performed on the isostructural  $\beta$ -phase showed identical predominant antiferromagnetic interactions.

It should be noted that interruption of the hydrogen-bonded network of the  $\alpha$ -phase, through the inclusion of guest solvent molecules, inverts the magnetic properties. The predominant ferromagnetic interactions found for the  $\alpha$ -phase have been transformed into very weak antiferro-



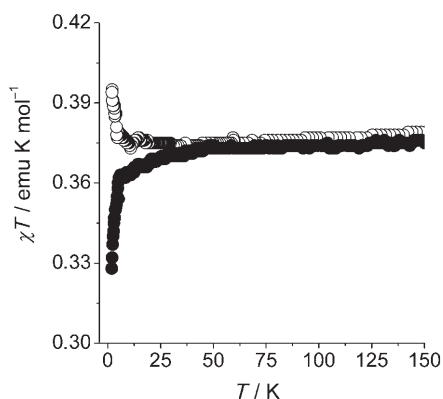


Figure 10. Comparison of the temperature dependence of  $\chi T$  product of a polycrystalline sample of porous  $\alpha$ -phase (○) and PTMTC·EtOH adduct (●) in the range of 1.8 to 150 K, measured with an applied magnetic field of 1000 Oe.

magnetic interactions for PTMTC·EtOH. Although the exact nature of these antiferromagnetic interactions has not been established, it is clear that the disruption of  $R_6(24)$  hexameric motifs by breaking two direct hydrogen bonds between PTMTC radicals prevents the propagation of ferromagnetic interactions along the planes, leading to the observation of predominant antiferromagnetic interactions.

The larger size compared to ethanol molecules and the ability to form hydrogen bonds of all other studied solvents prompted us to consider that inclusion of these molecules in the  $\alpha$ -phase may also induce the disruption of direct hydrogen bonds between PTMTC radicals and, therefore, a similar inversion on their magnetic properties. These expectations were confirmed by studying the magnetic properties of two of these adducts; the PTMTC·THF and PTMTC·2DMSO adducts. Magnetic measurements performed on both adducts showed them to exhibit very similar magnetic properties, with essentially paramagnetic behavior in the whole temperature range and the presence of very weak antiferromagnetic interactions at very low temperatures. Again, experimental magnetic data of both adducts were fit to the Curie–Weiss law with  $C=0.374$  and  $0.380 \text{ emu K mol}^{-1}$  and a Weiss constant of  $\theta=-0.3$  and  $-0.1 \text{ K}$ , respectively.

## Conclusion

This work demonstrates that a network based only on carboxylic–carboxylic hydrogen bonds can behave as a reversible dynamic open framework capable of showing solvato-magnetic effects. Thus, the proper self-assembly of stable polycarboxylic organic radicals can generate magnetic porous molecular materials with a purely organic character in which the carboxylic groups interact through hydrogen bonds generating a novel cyclic hexameric  $R_6(24)$  motif. The packing of such entities in the  $\alpha$ -phase defines the walls of the robust accessible tubular channels of 5 Å in diameter and serves as the pathway for the transmission of ferromag-

netic interactions between the unpaired spins of the radicals. At very low temperatures, the PTMTC  $\alpha$ -phase behaves as a soft magnet showing long-range magnetic ordering.

On the basis of its supramolecular character and high thermal stability, the hydrogen-bonded open framework of the  $\alpha$ -phase allows organic solvents with hydrogen-acceptor and/or -donor functionalities to be included that interact with the PTMTC radicals and, thereby, modify the overall magnetic properties. As a result, we observed a selective inclusion of polar organic solvents in the highly polar tubular channels, which induces structural rearrangements in the hydrogen-bonded network. The crystal transformations occurred so that solvent guest molecules located at the channels were hydrogen-bonded to the carboxylic groups of the PTMTC radicals, disrupting some direct hydrogen bonds between radicals. As expected, the interruption of direct bonds between PTMTC radicals induces large changes in the magnetic properties of the solid, yielding dominant ferromagnetic interactions in the  $\alpha$ -phase and predominant antiferromagnetic interactions in the corresponding adducts. The investigation of this solvato-magnetic effect is particularly relevant in the context of the newly emerging field of multifunctional porous materials.

## Experimental Section

All solvents were reagent grade from SDS and were used as received and distilled unless otherwise indicated. All reagents, organic and inorganic, were of high-purity grade and were obtained from E. Merck, Fluka Chemie, and Aldrich Chemical Co. Thin-layer chromatography (TLC) was performed on aluminum plates coated with Merck Silica gel 60. Elemental analyses were obtained from the Servei de Anàlisi de la Universitat Autònoma de Barcelona. The  $^1\text{H}$  NMR spectra were recorded on a Bruker ARX 250 spectrometer. FT-IR spectra were performed on a Perkin–Elmer Spectrum One spectrometer. Thermogravimetric analyses were performed under argon with a Perkin–Elmer TGA7 balance. X-ray powder diffraction (XRPD) experiments were recorded by using a diffractometer (INEL CPS-120) with Debye–Scherrer geometry.

**$\alpha\text{H}$ -(octadecachloro-4,4',4''-trimethyltriphenyl)methane (2):** A mixture of tris(2,3,5,6-tetrachlorophenyl)methane (**1**) (1.70 g, 2.58 mmol), chloroform (30 mL), and aluminum chloride (0.40 g, 3.00 mmol) was heated at 160 °C for 8 h in a glass pressure vessel. The mixture was then poured on to ice/1 N hydrochloric acid (50 mL) and was extracted with chloroform (2 × 50 mL). The organic mixture was washed with aqueous sodium hydrogen carbonate (100 mL) and water (100 mL). Immediately, the organic layer was filtered and the collected solid was washed with water and pentane to give **2** (2.22 g, 95% yield) as white powder.  $^1\text{H}$  NMR (250 MHz,  $\text{CDCl}_3$ ):  $\delta=7.1$  (s, 1H; CH), 7.7 ppm (s, 3H;  $\text{CHCl}_2$ ); IR (KBr):  $\tilde{\nu}=3040, 1540, 1390, 1368, 1350, 1303, 1271, 1139, 775, 713, 692, 485 \text{ cm}^{-1}$ ; elemental analysis calcd (%) for  $\text{C}_{22}\text{H}_4\text{Cl}_{18}$ : C 29.15, H 0.44; found: C 29.34, H 0.28.

**$\alpha\text{H}$ -(dodecachlorotriphenyl)methane-4,4',4''-tricarboxylic acid (3):** A mixture of **2** (0.55 g, 0.61 mmol) and 20% oleum (100 mL) was heated at 150 °C for 12 h. The final deep blue solution was cooled and poured onto crushed ice, and the collected solid was washed with water, dissolved in diethyl ether, and extracted with aqueous sodium hydrogen carbonate. The aqueous layer was acidified and extracted with diethyl ether. The extracted solid was recrystallized from  $\text{Et}_2\text{O}/n$ -pentane to give triacid **3** (0.44 g, 92% yield) as a white powder.  $^1\text{H}$  NMR (250 MHz,  $\text{CDCl}_3$ ):  $\delta=4.2$  (broad band, COOH), 7.1 ppm (s, 1H; CH); IR (KBr):  $\tilde{\nu}=3500\text{--}2500, 1721, 1556, 1331, 1300, 1274, 824, 795, 715, 664, 571, 472 \text{ cm}^{-1}$ ; ele-

mental analysis calcd (%) for  $C_{22}H_4O_6Cl_{12}$ : C 33.46, H 0.51; found: C 33.13, H 0.63.

**(Dodecachloro-4,4',4''-tricarboxytriphenyl)methyl radical (PTMTC):** A mixture of triacid **3** (0.25 g, 0.317 mmol) and powdered NaOH (0.7 g) was shaken with DMSO (30 mL) for 72 h in the dark. The mixture was filtered and iodine (0.093 g, 0.36 mmol) was added immediately into the resulting solution. The solution was left undisturbed in the dark for 30 min, after which it was washed with an aqueous solution of sodium hydrogen sulfite and then treated with  $Et_2O$ . Radical PTMTC was extracted with aqueous sodium hydrogen carbonate, and the aqueous layer was acidified and extracted with  $Et_2O$ . The solid extracted was recrystallized from  $Et_2O/n$ -pentane to give radical PTMTC (0.21 g, 85% yield) as red powder. IR (KBr):  $\tilde{\nu}$  = 3500–2500, 1740, 1694, 1662, 1537, 1441, 1408, 1352, 1326, 1290, 1251, 1226, 1040, 931, 752, 722, 665, 574, 522, 462  $cm^{-1}$ ; EPR ( $CH_2Cl_2$ ):  $g = 2.0019$ ,  $\Delta H^{13}C_{(w)} = 30.50$ ,  $\Delta H^{13}C_{(bridge)} = 12.70$ ,  $\Delta H^{13}C_{(ortho)} = 10.70$ ; ESI-TOF: 788.6  $[M]$ , 743.6  $[M-CO_2H]$ , 699.6  $[M-2CO_2H]$ , 663.7  $[M-2CO_2H-Cl]$ , 626.7  $[M-2CO_2H-2Cl]$ , 581.8  $[M-3CO_2H-2Cl]$ , 546.8  $[M-3CO_2H-3Cl]$ ; elemental analysis calcd (%) for  $C_{22}H_3O_6Cl_{12}$  (PORAOF-2): C 33.50, H 0.38; found: C 33.65, H 0.32; elemental analysis calcd (%) for  $C_{22}H_3O_6Cl_{12} \cdot EtOH \cdot H_2O$  ( $\beta$ -phase of PTMTC): C 33.81, H 1.29; found: C 33.64, H 1.34.

**EPR measurements:** EPR spectra were recorded on a Bruker ESP-300E spectrometer operating in the X-band (9.3 GHz). The signal-to-noise ratio was increased by accumulation of scans by using the F/F lock accessory to guarantee high-field reproducibility. Precautions to avoid undesirable spectral line broadening such as that arising from microwave power saturations and magnetic field over-modulation were taken. To avoid dipolar broadening, the solutions were carefully degassed three times by using vacuum cycles with pure Ar. The  $g$  values were determined against the DPPH standard ( $g = 2.0030$ ).

**Magnetic susceptibility measurements:** The temperature dependence of the static magnetic susceptibility has been measured with a MPMS2 SQUID magnetometer (Quantum Design) at different applied magnetic fields in the temperature range 1.8–300 K. The data were corrected for the contribution of the sample holder and for the diamagnetism of the sample estimated from the Pascal constants. The temperature dependence of magnetization and isothermal hysteresis curves for PORAOF-2 was measured down to 85 mK with a home-built dc susceptometer placed in a  $^3He/^4He$  dilution cryostat, capable of achieving temperatures of a few milliKelvin.

**X-ray crystal and molecular structural analyses:** X-ray single-crystal diffraction data for the  $\beta$ -phase of PTMTC were collected on a Nonius Kappa CCD diffractometer with an area detector and graphite-monochromated  $Mo_{K\alpha}$  radiation. X-ray diffraction data of single crystals were collected on a Kuma KM-8 diffractometer with a CCD area detector and silicon-monochromated synchrotron radiation ( $\lambda = 0.53378 \text{ \AA}$ ). The structures were solved by direct methods (SHELXS-97)<sup>[41]</sup> and refined with full-matrix least-squares procedures by using the program SHELXL-97. All non-hydrogen atoms were refined with anisotropic displacement parameters. The hydrogen atoms of the  $\alpha$ - and  $\beta$ -phase of PTMTC were found and refined isotropically. Because of a position disorder of one carboxylic group and the ethyl group of ethanol, hydrogen atoms for  $\beta$ -phase could not be exactly localized and were omitted. The structural conditions and details are listed in Table 1.

## Acknowledgements

This work was supported by Direcció General de Investigació (Spain), under project CONSOLIDER-C EMOCIONa (contract CTQ2006–06333/BQU) and Generalitat de Catalunya (2005 SGR-00591). We also thank the European Commission for the Marie Curie Research Training Network (contract QUEMOLNA, number MRTN-CT-2003–504880) and the NoE MAGMANet (contract NMP3-CT-2005–515767) and also to ESRF for providing synchrotron radiation beam time (experiment number CH-1236) on the ID.11 beam line. D.M. is grateful to the Generalitat de Catalunya for a predoctoral and postdoctoral grant. N.D. is also

grateful to the Ministerio de Educació y Ciencia (Spain) for the predoctoral grant No. AP2000–1842 of the FPU program. We thank Dr. Xavier Alcobé of the Unitat de Difracció de Raigs-X of Servei Científic-Tècnic of Universitat de Barcelona for X-ray powder diffraction measurements.

- a) S. Kitagawa, R. Kitaura, S. Noro, *Angew. Chem.* **2004**, *116*, 2388–2430; *Angew. Chem. Int. Ed.* **2004**, *43*, 2334–2375; b) O. M. Yaghi, M. O'Keefe, N. W. Ockwig, H. K. Chae, M. Eddaoudi, J. Kim, *Nature* **2003**, *423*, 705–714; c) B. Moulton, M. J. Zaworotko, *Chem. Rev.* **2001**, *101*, 1629–1658; d) M. Eddaoudi, D. B. Moler, H. Li, B. Chen, T. M. Reineke, M. O'Keefe, O. M. Yaghi, *Acc. Chem. Res.* **2001**, *34*, 319–330; e) R. Robson, *J. Chem. Soc. Dalton Trans.* **2000**, 3735–3744; f) M. J. Zaworotko, *Angew. Chem.* **2004**, *116*, 3180–3182; *Angew. Chem. Int. Ed.* **2000**, *39*, 3052–3054; g) A. Cheetham, G. Férey, T. Loiseau, *Angew. Chem.* **1999**, *111*, 3466–3492; *Angew. Chem. Int. Ed.* **1999**, *38*, 3269–3292; h) A. J. Blake, N. R. Champness, P. Hubberstey, M. Schröder, M. A. Withersby, *Coord. Chem. Rev.* **1999**, *183*, 117–138; i) C. N. R. Rao, S. Natarajan, R. Vaighyanathan, *Angew. Chem.* **2004**, *116*, 1490–1521; *Angew. Chem. Int. Ed.* **2004**, *43*, 1466–1496.
- a) M. Eddaoudi, J. Kim, N. Rosi, D. Vodak, J. Wachter, M. O'Keefe, O. M. Yaghi, *Science* **2002**, *295*, 469–472; b) H. Li, M. Eddaoudi, M. O'Keefe, O. M. Yaghi, *Nature* **1999**, *402*, 276–279.
- a) L. Pan, H. Liu, X. Huang, D. H. Olson, N. J. Turro, J. Li, *Angew. Chem.* **2003**, *115*, 560–564; *Angew. Chem. Int. Ed.* **2003**, *42*, 542–546; b) B. F. Abrahams, M. Moylan, S. D. Orchard, R. Robson, *Angew. Chem.* **2003**, *115*, 1892–1895; *Angew. Chem. Int. Ed.* **2003**, *42*, 1848–1851; c) B. Rather, M. J. Zaworotko, *Chem. Commun.* **2003**, 830–831; d) M. E. Kosal, J.-H. Chou, S. R. Wilson, K. S. Suslick, *Nat. Mater.* **2002**, *1*, 118–121; e) J. Sun, L. Weng, Y. Zhou, J. Chen, Z. Chen, Z. Liu, D. Zhao, *Angew. Chem.* **2002**, *114*, 4651–4653; *Angew. Chem. Int. Ed.* **2002**, *41*, 4471–4473; f) M. Eddaoudi, H. Li, O. M. Yaghi, *J. Am. Chem. Soc.* **2000**, *122*, 1391–1397.
- a) D. Maspocho, D. Ruiz-Molina, J. Veciana, *Chem. Soc. Rev.* **2007**, *36*, 770–818; b) C. J. Kepert, *Chem. Commun.* **2006**, 695–700; c) N. R. Champness, *Dalton Trans.* **2006**, 877–880.
- a) J. S. Seo, D. Whang, H. Lee, S. I. Jun, J. Oh, Y. J. Jeon, K. Kim, *Nature* **2000**, *404*, 982–986; b) Y. Cui, O. R. Evans, H. L. Ngo, P. S. White, W. Lin, *Angew. Chem.* **2002**, *114*, 6182–6185; *Angew. Chem. Int. Ed.* **2002**, *41*, 1159–1162; c) O. R. Evans, H. L. Ngo, W. Lin, *J. Am. Chem. Soc.* **2001**, *123*, 10395–10396; d) H. L. Ngo, W. Lin, *J. Am. Chem. Soc.* **2002**, *124*, 14298–14299; e) Y. Cui, S. J. Lee, W. Lin, *J. Am. Chem. Soc.* **2003**, *125*, 6014–6015.
- a) J. A. Hanko, M. G. Kanatzidis, *Angew. Chem.* **1998**, *110*, 354–356; *Angew. Chem. Int. Ed.* **1998**, *37*, 342–344; b) A. E. C. Palmqvist, B. B. Iversen, E. Zanghellini, M. Behm, G. D. Stucky, *Angew. Chem.* **2004**, *116*, 718–722; *Angew. Chem. Int. Ed.* **2004**, *43*, 700–704.
- a) P. Feng, *Chem. Commun.* **2001**, 1668–1669; b) J.-C. Dai, X.-T. Wu, Z.-Y. Fu, C.-P. Cui, S.-M. Hu, W.-X. Du, L.-M. Wu, H.-H. Zhang, R.-Q. Sun, *Inorg. Chem.* **2002**, *41*, 1391–1396.
- D. Maspocho, D. Ruiz-Molina, J. Veciana, *J. Chem. Mater.* **2004**, *14*, 2713–2723.
- S. Kitagawa, K. Uemura, *Chem. Soc. Rev.* **2005**, *34*, 109–119.
- N. Guillou, C. Livage, M. Drillon, G. Férey, *Angew. Chem.* **2003**, *115*, 5472–5475; *Angew. Chem. Int. Ed.* **2003**, *42*, 5314–5317.
- a) K. Barthelet, J. Marrot, D. Riou, G. Férey, *Angew. Chem.* **2002**, *114*, 291–294; *Angew. Chem. Int. Ed.* **2002**, *41*, 281–284; b) S. S.-Y. Chui, S. M.-F. Lo, J. P. H. Charmant, A. G. Orpen, I. D. Williams, *Science* **1999**, *283*, 1148–1150.
- a) J. N. Behera, G. Paul, A. Choudhury, C. N. R. Rao, *Chem. Commun.* **2004**, 456–457; b) B. Moulton, J. Lu, R. Hajndl, S. Hariharan, M. J. Zaworotko, *Angew. Chem.* **2002**, *114*, 2945–2948; *Angew. Chem. Int. Ed.* **2002**, *41*, 2821–2824.
- G. J. Halder, C. J. Kepert, B. Moubarak, K. S. Murria, J. D. Cashion, *Science* **2002**, *298*, 1765.
- A. Rujiwatra, C. J. Kepert, M. J. Rosseinsky, *Chem. Commun.* **1999**, 2307–2308.

- [15] a) L. G. Beauvais, J. R. Long, *J. Am. Chem. Soc.* **2002**, *124*, 12096–12097; b) M. Kurmoo, H. Kumagai, S. M. Hugues, C. J. Kepert, *Inorg. Chem.* **2003**, *42*, 6709–6722; c) C. Livage, C. Egger, M. Nogues, G. Férey, *J. Mater. Chem.* **1998**, *8*, 2743–2747.
- [16] a) K. Uemura, S. Kitagawa, K. Fukui, K. Saito, *J. Am. Chem. Soc.* **2004**, *126*, 3817–3828; b) T. Kumar Maji, K. Uemura, H.-C. Chang, R. Matsuda, S. Kitagawa, *Angew. Chem.* **2004**, *116*, 3331–3334; *Angew. Chem. Int. Ed.* **2004**, *43*, 3269–3272; c) K. Uemura, S. Kitagawa, M. Kondo, K. Fukui, R. Kitaura, H.-C. Chang, T. Mizutani, *Chem. Eur. J.* **2002**, *8*, 3586–3600.
- [17] a) K. Biradha, M. Fujita, *Angew. Chem.* **2002**, *114*, 3542–3545; *Angew. Chem. Int. Ed.* **2002**, *41*, 3392–3395; b) K. Biradha, Y. Hongo, M. Fujita, *Angew. Chem.* **2002**, *114*, 3545–3548; *Angew. Chem. Int. Ed.* **2002**, *41*, 3395–3398.
- [18] a) E. Y. Lee, S. Y. Jang, M. P. Suh, *J. Am. Chem. Soc.* **2005**, *127*, 6374–6381; b) H. J. Choi, M. P. Suh, *J. Am. Chem. Soc.* **2004**, *126*, 15844–15851; c) E. Y. Lee, M. P. Suh, *Angew. Chem.* **2004**, *116*, 2858–2861; *Angew. Chem. Int. Ed.* **2004**, *43*, 2798–2801; d) M. P. Suh, J. W. Ko, H. J. Choi, *J. Am. Chem. Soc.* **2002**, *124*, 10976–10977.
- [19] a) Z. Wang, B. Zhang, H. Fujiwara, H. Kobayashi, M. Kurmoo, *Chem. Commun.* **2004**, 416–417; b) M. Kurmoo, H. Kumagai, M. Akita-Tanaka, K. Inoue, S. Takagi, *Inorg. Chem.* **2006**, *45*, 1627–1637.
- [20] M. Kurmoo, H. Kumagai, K. W. Chapman, C. J. Kepert, *Chem. Commun.* **2005**, 3012–3014.
- [21] a) S.-I. Ohkoshi, K.-I. Arai, Y. Sato, K. Hashimoto, *Nat. Mater.* **2004**, *3*, 857–861; b) Y. Sato, S.-I. Ohkoshi, K.-I. Arai, M. Tozawa, K. Hashimoto, *J. Am. Chem. Soc.* **2003**, *125*, 14590–14595.
- [22] D. Maspocho, D. Ruiz-Molina, K. Wurst, N. Domingo, M. Cavallini, F. Biscarini, J. Tejada, C. Rovira, J. Veciana, *Nat. Mater.* **2003**, *2*, 190–195.
- [23] For purely organic porous materials with a robust structure in the absence of solvent molecules, see: a) B. T. Ibragimov, S. A. Talipov, T. F. Aripov, *J. Inclusion Phenom. Mol. Recognit. Chem.* **1994**, *17*, 317–324; b) A. T. Ung, D. Gizachew, R. Bishop, M. L. Scudder, I. G. Dance, D. C. Craig, *J. Am. Chem. Soc.* **1995**, *117*, 8745–8756; c) P. Brunet, M. Simard, J. D. Wuest, *J. Am. Chem. Soc.* **1997**, *119*, 2737–2738; d) P. Sozzani, A. Comotti, R. Simonutti, T. Meersmann, J. W. Logan, A. Pines, *Angew. Chem.* **2000**, *112*, 2807–2810; *Angew. Chem. Int. Ed.* **2000**, *39*, 2695–2699; e) O. Saied, T. Maris, X. Wang, M. Simard, J. D. Wuest, *J. Am. Chem. Soc.* **2005**, *127*, 10008–10009; f) N. Malek, T. Maris, M. Simard, J. D. Wuest, *J. Am. Chem. Soc.* **2005**, *127*, 5910–5916.
- [24] For a zeolite-like purely organic porous material, see: T. Hertzsch, F. Budde, E. Weber, J. Hulliger, *Angew. Chem.* **2002**, *114*, 2385–2388; *Angew. Chem. Int. Ed.* **2002**, *41*, 2281–2284.
- [25] For a dynamic structural purely organic porous material, see: K. Endo, T. Sawaki, M. Koyanagi, K. Kobayashi, H. Masuda, Y. Aoyama, *J. Am. Chem. Soc.* **1995**, *117*, 8341–8352.
- [26] a) D. Maspocho, N. Domingo, D. Ruiz-Molina, K. Wurst, J. Tejada, C. Rovira, J. Veciana, *J. Am. Chem. Soc.* **2004**, *126*, 730–731; b) N. Roques, D. Maspocho, N. Domingo, D. Ruiz-Molina, K. Wurst, J. Tejada, C. Rovira, J. Veciana, *Chem. Commun.* **2005**, 4801–4803; c) N. Roques, D. Maspocho, K. Wurst, D. Ruiz-Molina, C. Rovira, J. Veciana, *Chem. Eur. J.* **2006**, *12*, 9238–9253.
- [27] a) D. Maspocho, N. Domingo, D. Ruiz-Molina, K. Wurst, J. M. Hernández, G. Vaughan, C. Rovira, F. Lloret, J. Tejada, J. Veciana, *Chem. Commun.* **2005**, 5035–5037; b) D. Maspocho, D. Ruiz-Molina, K. Wurst, C. Rovira, J. Veciana, *Chem. Commun.* **2004**, 1164–1165.
- [28] M. Ballester, *Acc. Chem. Res.* **1985**, *18*, 380–387.
- [29] D. Maspocho, P. Gerbier, L. Catala, J. Vidal-Gancedo, K. Wurst, C. Rovira, J. Veciana, *Chem. Eur. J.* **2002**, *8*, 3635–3645.
- [30] A preliminary communication of this work has already been published: D. Maspocho, N. Domingo, D. Ruiz-Molina, K. Wurst, G. Vaughan, J. Tejada, C. Rovira, J. Veciana, *Angew. Chem.* **2004**, *116*, 1864–1868; *Angew. Chem. Int. Ed.* **2004**, *43*, 1828–1832.
- [31] M. Ballester, J. Riera, J. Castañer, C. Rovira, O. Armet, *Synthesis* **1986**, 64–66.
- [32] O. Armet, J. Veciana, C. Rovira, J. Riera, J. Castaner, E. Molins, J. Rius, C. Miravittles, S. Olivella, J. Brichtfeus, *J. Phys. Chem.* **1987**, *91*, 5608–5616.
- [33] L. Leiserowitz, *Acta Crystallogr. Sect. B* **1976**, *32*, 775–802.
- [34] J. N. Moorthy, R. Natajaran, P. Mal, P. Venugopalan, *J. Am. Chem. Soc.* **2002**, *124*, 6530–6531.
- [35] S. Kuduva, D. C. Craig, A. Nangia, G. R. Desiraju, *J. Am. Chem. Soc.* **1999**, *121*, 1936–1944.
- [36] S. V. Kolotuchin, E. E. Fenlon, S. R. Wilson, C. J. Lowth, S. C. Zimmerman, *Angew. Chem.* **1995**, *107*, 2873–2876; *Angew. Chem. Int. Ed. Engl.* **1995**, *34*, 2654–2657.
- [37] a) A. Franken, C. A. Kilner, J. D. Kennedy, *Chem. Commun.* **2004**, 328–329; b) A. Franken, M. J. Carr, W. Clegg, C. A. Kilner, J. D. Kennedy, *Dalton Trans.* **2004**, 3552–3561; c) A. Uchida, M. Hasewaga, H. Manami, *Acta Crystallogr. Sect. C* **2003**, *59*, O435–O438; d) J. Canonne, G. Nowogrocki, J.-C. Boivin, D. Thomas, *Acta Crystallogr. Sect. B* **1980**, *36*, 2664–2667; e) J. A. Kanters, G. Roelofsen, *Acta Crystallogr. Sect. B* **1976**, *32*, 3328–3331; f) L. M. Shkolnikova, T. N. Safonova, M. A. Poraikoshits, N. M. Dyatlova, J. Podlaha, *Zh. Strukt. Khim.* **1982**, *23*, 569–573; g) J. Canonne, J.-C. Boivin, G. Nowogrocki, D. Thomas, *Acta Crystallogr. Sect. B* **1978**, *34*, 3233–3237.
- [38] Elemental analysis calcd (%) for C<sub>22</sub>H<sub>3</sub>O<sub>6</sub>Cl<sub>12</sub> (P<sub>4</sub>OROF-2, RT): C 33.50, H 0.38; found (RT): C 33.65, H 0.32; found (265°C): C 33.80, H 0.52.
- [39] K. Kobayashi, A. Sato, S. Sakamoto, K. Yamaguchi, *J. Am. Chem. Soc.* **2003**, *125*, 3035–3045.
- [40] For examples of purely organic ferromagnets, see: a) M. Tamura, Y. Nakazawa, D. Shiomi, K. Nozawa, Y. Hosokoshi, M. Ishikawa, M. Takahashi, M. Kinsohita, *Chem. Phys. Lett.* **1991**, *186*, 401–404; b) A. Caneschi, F. Ferraro, D. Gatteschi, A. Le Lirzin, M. A. Novak, E. Rentscher, R. Sessoli, *Adv. Mater.* **1995**, *7*, 476–478; c) T. Nogami, K. Tomioka, T. Ishida, H. Yoshikawa, M. Yasui, F. Iwasaki, H. Iwamura, N. Takeda, M. Ishikawa, *Chem. Lett.* **1994**, 29–32; d) R. Chiarelli, M. A. Novak, A. Rassat, J. L. Tholance, *Nature* **1993**, *363*, 147–149; e) P. M. Allemand, K. C. Khermani, A. Koch, F. Wudl, K. Holczer, S. Donovan, G. Grüner, J. D. Thompson, *Science* **1991**, *253*, 301–303; f) W. Fujita, K. Awaga, *Chem. Phys. Lett.* **2002**, *357*, 385–388; g) A. Alberola, R. J. Less, C. M. Pask, J. M. Rawson, F. Palacio, P. Oliete, C. Paulsen, A. Yamaguchi, R. D. Farley, D. M. Murphy, *Angew. Chem.* **2003**, *115*, 4930–4933; *Angew. Chem. Int. Ed.* **2003**, *42*, 4782–4785.
- [41] G. M. Sheldrick, SHELXL-97, Program for Crystal Structure refinement, University of Göttingen, Göttingen (Germany), **1997**.

Received: March 2, 2007  
Published online: July 16, 2007